IEEE Access
Multidisciplinary | Rapid Review | Open Access Journal

Received April 13, 2021, accepted May 11, 2021, date of publication May 17, 2021, date of current version May 24, 2021.

Digital Object Identifier 10.1109/ACCESS.2021.3081354

An E-Band Beam Sharpening Antenna Based on Monopulse Comparator

ZHENHUA CHEN[1,2], (Member, IEEE), PENG TENG[1], (Graduate Student Member, IEEE), AND JIANRU WANG[1], (Graduate Student Member, IEEE)

[1]Institute of Radar Technology, Nanjing University of Information Science and Technology, Nanjing 210044, China
[2]Collaborative Innovation Center on Forecast and Evaluation of Meteorological Disasters, Nanjing University of Information Science and Technology, Nanjing 210044, China

Corresponding author: Zhenhua Chen (zhchen@nuist.edu.cn)

ABSTRACT An E-band antenna module and corresponding beam sharpening method is proposed to achieve high azimuth resolution for front-looking real aperture radar application. To achieve high angular resolution with a small antenna aperture size, a solution involving real beam and super-resolution is investigated. A monopulse antenna is developed to produce two coprime channels, which are essential for the subsequent beam sharpening in digital domain. A dual-aperture horn antenna and a monopulse comparator that make up the monopulse antenna are designed respectively, and the experimental prototypes are fabricated and tested. Experimental results show the antenna module can operate in the 75 to 80 GHz band, more than 20 dBi gain and 12° half power azimuth beamwidth can be maintained in the sum-patterns, and the null-depths are lower than −20 dB in the difference-patterns. Based on the measured sum and difference patterns, an azimuth super-resolution processing based on two-channel deconvolution is implemented. The simulation results show the sharpening ratio can achieve 12 dB with 0 dB signal-noise-ratio and truncated half power beamwidth. Theoretically, the azimuth super-resolution of 0.8° can be achieved with 20 mm aperture size. The corresponding achievements are valuable in the follow-up E-band civil front-looking imaging system.

INDEX TERMS E-band antenna, monopulse comparator, high angular resolution, super-resolution.

I. INTRODUCTION

In the entire E-band frequency range (60 to 90 GHz), the 77 GHz frequency band has been released to civilian use in many countries [1]–[5]. A large number of 77G-radar-based application scenarios are gradually emerging. At the early stage, the application of 77 GHz band is mainly driven by the advanced driver assistance system (ADAS) [6], [7]. Thanks to the development of highly integrated silicon germanium (SiGe) single-chip radar transceiver [8], [9], numerous applications come true, for instance, perimeter intrusion detection, airport runway foreign object debris detection, life signs monitoring, intelligent traffic system, and so on [10]–[15]. In all the applications, range resolution and angular resolution are two important indexes of radar systems. By transmitting signals with wide bandwidth and pulse compression technology, radars can obtain high range resolution. However, angular resolution varies due to different radar systems. The angular resolution of real aperture radar (RAR) is limited by the antenna aperture size, and decreases dramatically with the increase of detection distance. Doppler beam sharpening (DBS) and synthetic aperture radar (SAR) are widely used to improve the angular resolution by making use of relative motion between radar and targets, but both of the two system architectures are usually complex and costly. Moreover, there are blind areas of front-looking detecting when the DBS and SAR technologies are adopted, which greatly limits the application in some fields [16]–[19]. In addition to the DBS and SAR systems, some super-resolution direction of arrival (DOA) solutions, such as multiple signal classification (MUSIC) and improved root MUSIC algorithms are proposed to increase the angular resolution, but a certain scale of array elements and enough signal-noise-ratio (SNR) are required to implement these technologies [20], [21]. Overall, considering the cost performance, especially of the civil radar products, the traditional RARs are still primary choice for front-looking imaging application [22], and improve the angular resolution

The associate editor coordinating the review of this manuscript and approving it for publication was Abhishek K. Jha.

This work is licensed under a Creative Commons Attribution 4.0 License. For more information, see https://creativecommons.org/licenses/by/4.0/

of RARs with a limited aperture size has always been an attractive research topic.

The motivation of the work mentioned in this paper is to develop the antenna module of an E-band radar sensor that can realize 360° azimuth coverage with adequate range resolution and azimuth resolution, simultaneously. The radar sensor features the separate transmitting and receiving antennas, and works in frequency modulated continuous wave (FMCW) mode, therefore, the range resolution ΔR can be achieved by selecting the appropriate modulation bandwidth,

$$\Delta R = \sigma \cdot \frac{C}{2B} \tag{1}$$

where C is light speed, B is modulation bandwidth, and σ is a coefficient that depends on the windowing function in signal processing, which is usually taken as 1.2 [23]. Considering the required range resolution of 40 mm and the working frequency range of the transceiver, the working range of antenna module is established as 75 to 80 GHz. In azimuth, mechanical scanning of real beam is selected to achieve 360° coverage. The work presented in this paper focuses on how to achieve the azimuth resolution of 1° with receiving antenna. As for the receiving antenna, there are several choices. If a conventional parabolic antenna is adopted and the angular resolution is achieved only by the beamwidth, the aperture size can be estimated by the following empirical formula,

$$\theta_{HPBW} = 70 \cdot \frac{\lambda}{D} \tag{2}$$

where λ is wavelength, θ_{HPBW} is half power beamwidth (HPBW), and D is diameter of parabolic [24]. Given the required θ_{HPBW} is 1°, the value of D is about 280 mm, which is a relatively large size, and the requirements for the radome and servo would be correspondingly high. In order to reduce the complexity and cost of the radar sensor, a small aperture antenna would be preferred, therefore, the main challenge is how to achieve high azimuth resolution with a small aperture.

A concept has been widely accepted that the received azimuth echoes of RARs are the convolution of azimuth sampling sequence of antenna beam and distribution function of target reflectivity. Therefore, in theory, as long as a proper deconvolution factor can be constructed, the azimuth information of target can be reconstructed by deconvolution, even though the receiving antenna features a wide azimuth beam [25], [26]. In other words, the azimuth beamwidth is compressed by deconvolution without increase the aperture size of antenna. This is so-called beam sharpening effect. Because of the band-pass characteristics of a single antenna pattern in Fourier domain, there are transmission zeros in spatial Fourier transform of pattern, small changes in noise can make deconvolution infeasible, therefore, multi-channel deconvolution is proposed to eliminate the ill-posed deconvolution factor in single receiving channel. In all the multi-channel solutions, the monopulse radar is considered a good candidate, since it has two coprime channels, named sum channel and difference channel. The monopulse radar is usually used for precise tracking and features high angle measurement accuracy, while its angular resolution is dominated by the beamwidth of sum beam, that is to say, if multiple targets exist in the main beam range, they cannot be distinguished simultaneously. By deconvolution-based beam sharpening, the beamwidth can be compressed and its angular resolution can be improved.

In this work, we first demonstrate the system composition of beam sharpening antenna module, and then a compact E-band monopulse comparator (MPC) adapted to a dual-aperture horn antenna is shown. The proposed comparator overcomes the complexity of structure and the inconsistent orientation of the waveguide ports of the traditional comparators, presents good performance of amplitude and phase balance characteristics, thus the radiation patterns with enough null-depths can be realized. Based on the measured sum patterns and difference patterns in azimuth, the subsequent beam sharpening is carried out in digital domain without any change to the hardware. The performance of beam sharpening is given and discussed in the last section and the effectiveness of the proposed beam sharpening antenna is verified.

II. BEAM SHARPENING ANTENNA FRAMEWORK

The beam sharpening antenna proposed in this paper is composed of a dual-aperture horn antenna and a monopulse sum and difference comparator in hardware. The ability of beam sharpening depends not only on hardware, but also on subsequent signal processing. The system framework is illustrated in Fig. 1.

The receiving antenna features two radiating apertures (aperture 1 and aperture 2) close to each other, thus two overlapping wide beams in azimuth can be generated, which is necessary for monopulse system. The echoes reflected from targets are received by the two apertures, and then separated into two parts by the sum and difference comparator network. Once the receiving antenna and the comparator are established, the sum and difference patterns in azimuth can be measured exactly, and the coprime deconvolution factors of sum and difference channels can be constructed, respectively. Based on the received echoes and the corresponding deconvolution factors, the beam sharpening effect can be achieved, this is equivalent to the realization of azimuth super-resolution. The detailed design process and performance evaluation about each functional module will be provided in the following sections.

III. DESIGN OF THE MONOPULSE ANTENNA

A. DUAL-APERTURE HORN ANTENNA

According to the framework illustrated in Fig. 1, the beam sharpening antenna needs two overlapping beams in azimuth. In the desired frequency range (75 to 80 GHz), parabolic antenna, printed circuit board (PCB) based antenna and horn antenna are often used. The parabolic antenna is usually used to generate a narrow beam but a separate feed source is necessary, which result in a high profile and complex structure,

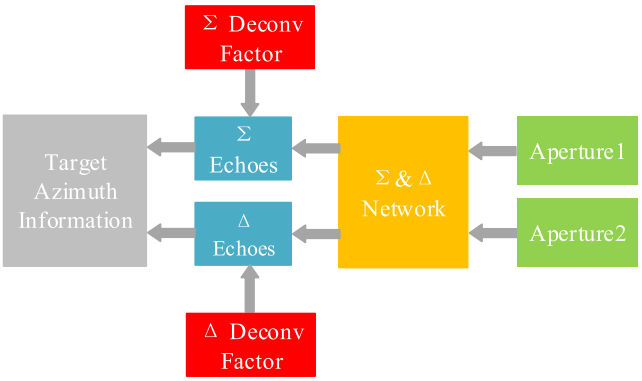

FIGURE 1. Framework of the proposed beam sharpening antenna module.

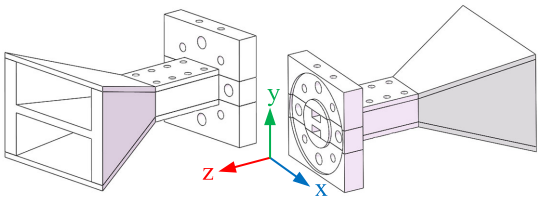

FIGURE 2. Structure diagram of the dual-aperture antenna.

what's more, narrow beam is not essential in this work. The PCB-based antenna is another choice, but the power loss over E-band is relatively high, and the high frequency interfaces of the radar transceiver are waveguide flanges. Based on the above mentioned considerations, a dual-aperture horn antenna is adopted, the structure diagram is shown in Fig. 2. It can be found the two apertures are formed by a simple sandwich structure and separated with a common 1.5 mm thick metal partition wall. The length and width of each aperture is 20 mm and 8 mm, respectively. Two standard WR12 waveguide ports are arranged symmetrically on a single UG-387/U flange.

Assumed the two apertures are fed with ideal in-phase or anti-phase signals with equal magnitude, the simulated sum (Σ) and difference (Δ) radiation patterns of two orthogonal H- and E-planes are shown in Fig. 3 and Fig. 4, respectively. The H-plane corresponds to x-o-z plane shown in Fig. 2, while the E-plane corresponds to y-o-z plane.

As presented in Fig. 3 and Fig. 4, the simulated gain of the dual-aperture antenna is about 20 dBi at 77 GHz, the HPBW of the sum and difference patterns in H- and E-plane is 18° and 12°, respectively. The first side lobe of E-plane is about −10 dB, and the null-depth is about −50 dB. The patterns of E-plane will be adopted as the azimuth patterns in final application. It should be noticed when the two antenna elements are excited in antiphase, the symmetry of the electric field distribution on the radiation aperture is much better than that of the magnetic field distribution. Therefore, it can be found the null point of E-plane is much steeper than that of H-plane, and the null-depth level will be greatly affected by the phase difference between the two antennas' feed signals.

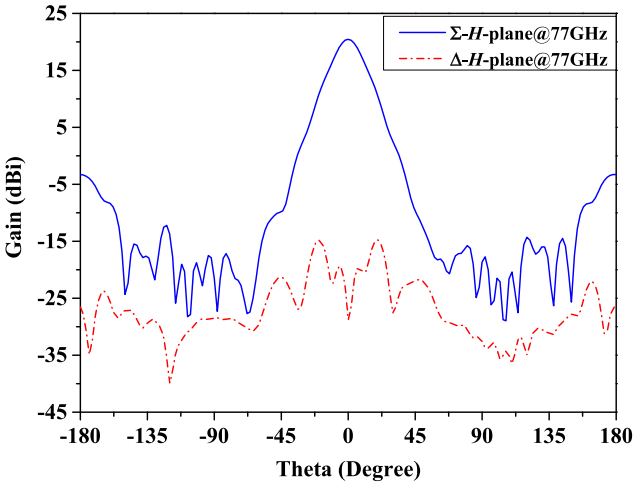

FIGURE 3. Simulated sum and difference patterns in the *H*-plane of the dual-aperture antenna.

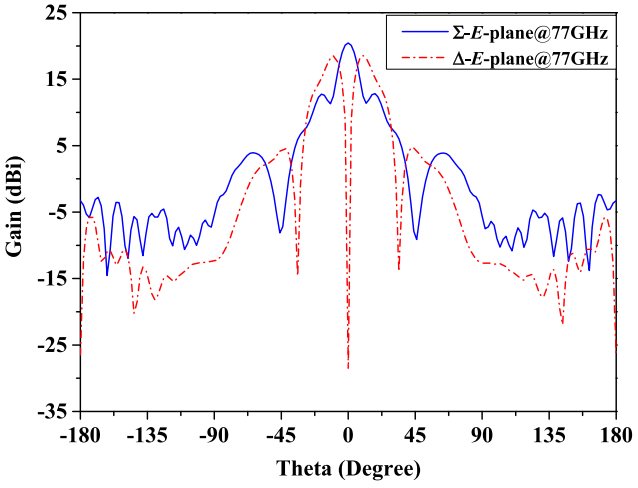

FIGURE 4. Simulated sum and difference patterns in the *E*-plane of the dual-aperture antenna.

B. PLANAR MONOPULSE COMPARATOR

The MPCs can be realized with PCB-based micro-strip line solutions, substrate integrated waveguide (SIW) solutions, metal waveguide solutions, or monolithic integrated circuits solutions [27]–[30]. Considering the low loss in millimeter wave frequencies, waveguide solutions are usually preferred.

The traditional waveguide MPCs are almost realized based on Magic-T structures, which are inherently low loss and broadband. However, the four ports of Magic-T point to four different directions, and the two input ports are orthogonal to the sum and difference ports. Additionally, to reduce the input reflection and improve the output phase balance, a hybrid tee is often needed in the center of Magic-T structure, all of which lead to the structural complexity [31].

The adopted MPC is designed based on a Riblet short slot hybrid coupler, which would lead in a 90° phase difference. Since a MPC is often consists of in-phase and reversed-phase paths, the remaining 90° phase difference is

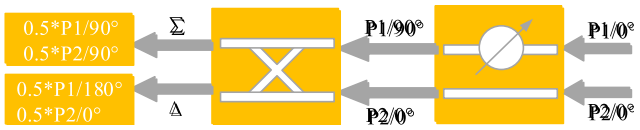

FIGURE 5. Schematic of the proposed monopulse comparator.

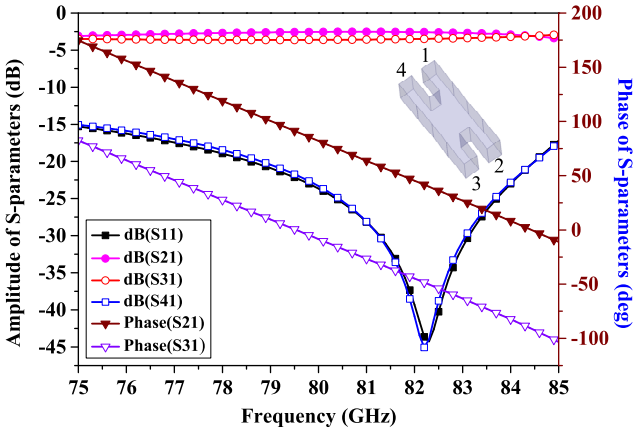

FIGURE 6. Simulated S-parameters of the Riblet short slot coupler.

introduced with a 90° phase shifter. These two functional parts are designed independently and combined for further optimization.

A schematic of the proposed MPC is shown in Fig. 5. It consists of a Riblet quadrature coupler and a 90° phase shifter. Two signals delivered by two similar antennas are fed into the two ports of MPC (P1 and P2), 90° phase difference is generated between the two signals after they pass through a 90° phase shifter. Then, the two quadrature signals are combined with a 3 dB Riblet short slot coupler, which will introduce another 90° phase difference. Finally, the two signals from antennas are combined in phase and out of phase, and delivered to the sum (Σ) and difference (Δ) ports, respectively.

Most quadrature hybrids are realized using multi-section branch guide coupler, this kind of couplers can provide low loss and large frequency coverage, while the structure dimensions bring great challenges to the capability of machining. The E-plane Riblet short slot coupler is chosen in this paper for its simple machining and compact size. Fig. 6 gives the simulated S-parameters curves.

It can be found, the Riblet coupler covers the 75 to 85 GHz band with the nominal amplitude and phase imbalance better than 0.6 dB and 0.5°, respectively, and with an input return loss better than 15 dB.

As the above mentioned, in addition to the Riblet coupler, another phase shifter is needed to provide additional 90° phase shift. Due to the dispersion effect, it is difficult to achieve a certain phase shift in a wide bandwidth based on a conventional waveguide structure [32]. Here, a stub-loaded topology is adopted, as shown in Fig. 7. The simulated performance show that the phase difference between the two

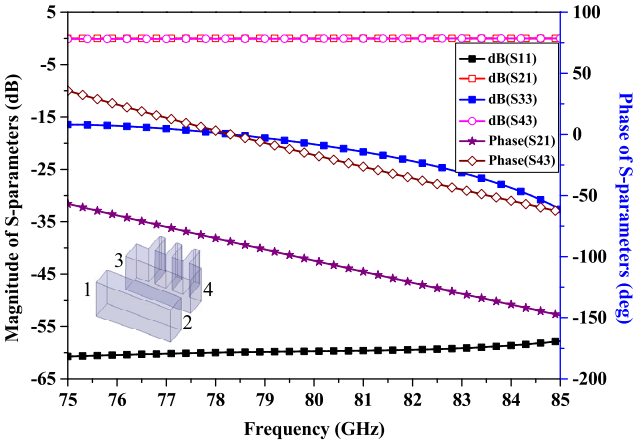

FIGURE 7. Simulated S-parameters of the stub-loaded phase shifter.

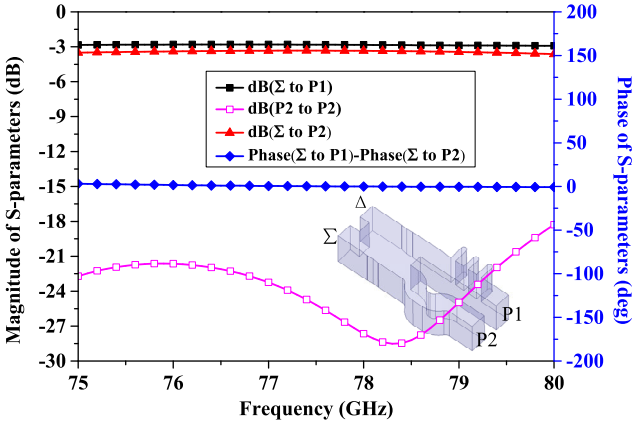

FIGURE 8. Simulated results of sum channel of the proposed monopulse comparator.

branches (port 1-2 and port 3-4) are 90° while the return loss and insertion loss meet the design requirement.

Based on the Riblet coupler and stub-loaded phase shifter, the model of the MPC is established. Fig. 8 and Fig. 9 depict the simulated S-parameters of the difference channel (Δ-channel) and sum channel (Σ-channel). The maximum amplitude imbalance is about 0.7 dB, and the phase imbalance is better 4°. The simulation results clearly show that when two similar signals are fed into port1 (P1) and port2 (P2), they are combined in-phase and output from Σ-port, while cancelled out of phase and output from Δ-port. The generated sum and difference signals are greatly affected by the balance of amplitude and phase.

C. MEASUREMENT OF THE MONOPULSE ANTENNA PATTERNS

To obtain the radiation patterns of the proposed monopulse antenna, the prototypes of dual-aperture horn and MPC are machined with standard CNC process. As shown in Fig. 10, the interface between the antenna and MPC is UG-387/U flange with two WR12 waveguide ports. Therefore, the MPC adapted to antenna cannot be measured directly by VNA with standard test interfaces.

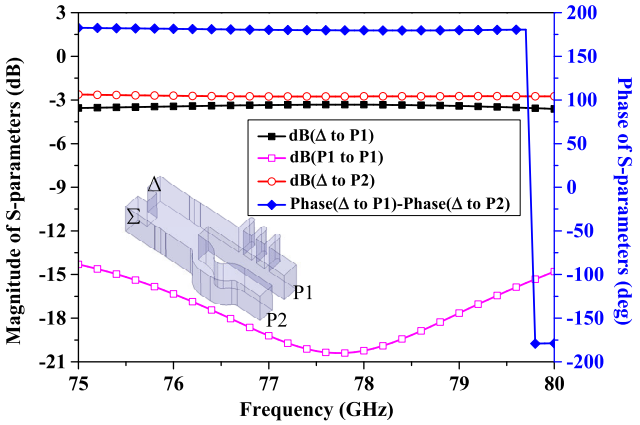

FIGURE 9. Simulated results of difference channel of the proposed monopulse comparator.

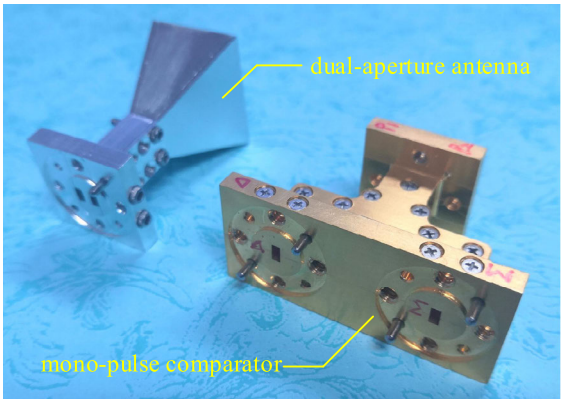

FIGURE 10. Assembled dual-aperture antenna and monopulse comparator.

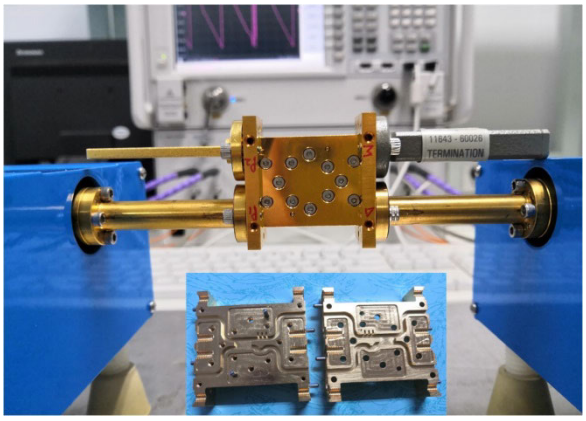

FIGURE 11. Measurement setup of the developed monopulse comparator and the inner structure of the fabricated module.

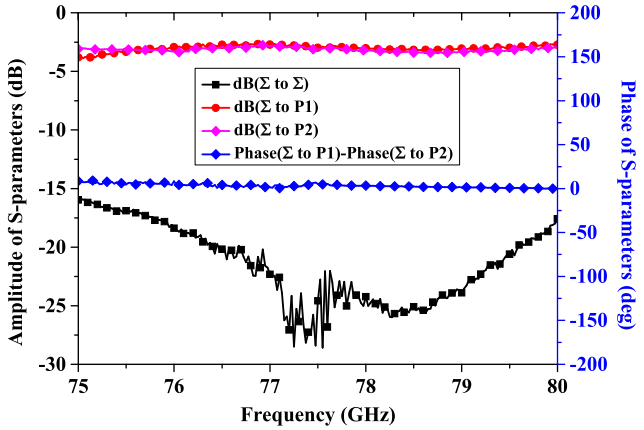

FIGURE 12. Measured results of sum channel of the proposed monopulse comparator.

To verify the performance of the MPC, a similar MPC module with the same internal structure but four independent standard waveguide flanges is fabricated. Fig. 11 demonstrates the inner view of the MPC under test, and the measurement setup.

The measurement instrument is Keysight N5264A vector network analyzer (VNA) and OML V10VNA2-T/R frequency extenders. As mentioned above, the MPC prototype is designed to cover 75 to 80 GHz with WR12 waveguide ports, while the test interface of the instrument is WR10 waveguide ports. During the test, two ports of the MPC are connected with the two frequency extenders, while the other two ports are terminated with fixed waveguide load. The performance of sum channel and difference channel is measured and given in Fig. 12 and Fig. 13, respectively. In both sum and difference channels, the operational bandwidth of Port Σ and Δ can cover from 75 to 80 GHz with return loss larger than 15 dB. The maximum amplitude imbalance is about 0.8 dB at low frequency end, and the phase imbalance is better than 9° and 13°, respectively. Comparing the simulated results shown in Fig. 8 and 9 with the measured results shown in Fig 12 and 13, it can be found the results are basically consistent, the small difference may be caused by the inconsistency of the interface between the MPC and test instrument.

Far-field performance of the monopulse antenna has been measured in a microwave compact range anechoic chamber, as shown in Fig. 14. The sum-patterns at 77 GHz of the monopulse antenna in the E- and H-plane are presented in Fig. 15. It can be seen that 12° HPBW of azimuth pattern can be achieved, where the first side-lobe levels are around −10 dB and cross polarizations are better than −29 dB. Fig. 16 shows the difference-patterns at 77 GHz in the E- and H-plane. The null-depth level for the E-plane difference pattern is as low as −27 dB. These results indicate the proposed monopulse comparator display good signal comparison capability for the monopulse antenna in the desired azimuth plane.

It should be noted that the real beamwidth of the sum pattern is not narrow enough to achieve the desired azimuth resolution of 1°. Therefore, a further beam sharpening is required and would be given in the next section. Fig. 17 gives the measured gain and null-depth levels of azimuth sum- and difference-patterns, respectively. In the entire working frequency band, more than 20 dBi gain can be maintained in the sum-patterns, while the gain of difference-patterns is about

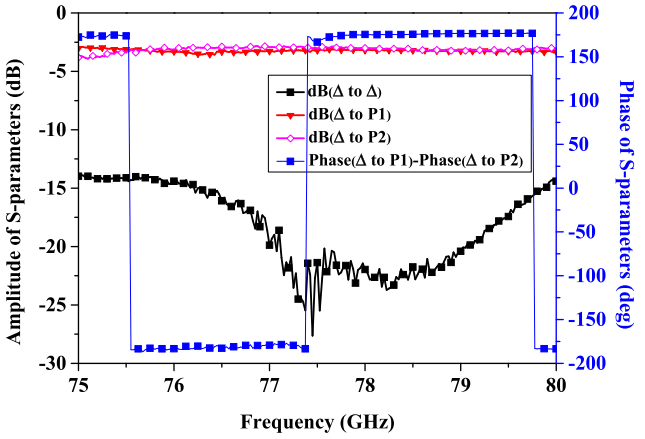

FIGURE 13. Measured results of difference channel of the proposed monopulse comparator.

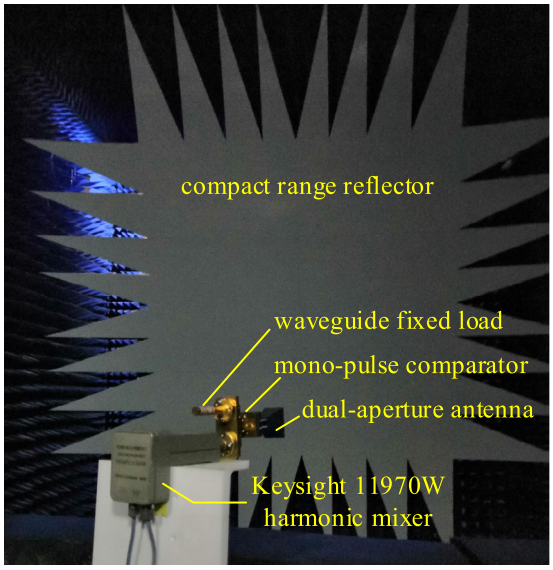

FIGURE 14. The compact range test scene of the developed monopulse antenna.

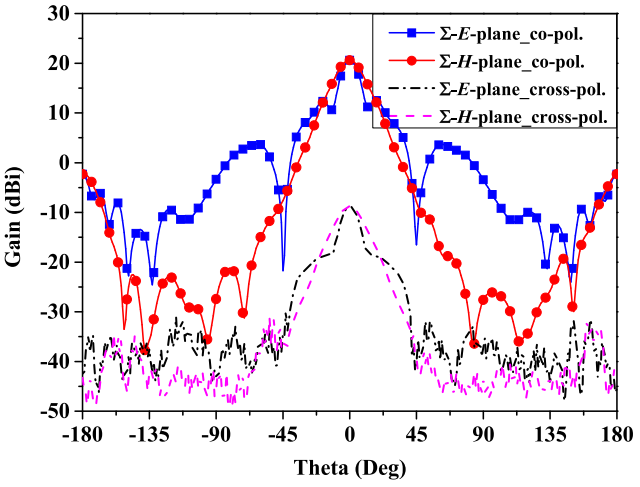

FIGURE 15. Measured sum-patterns of azimuth plane (*E*-plane) and elevation plane (*H*-plane) at 77 GHz.

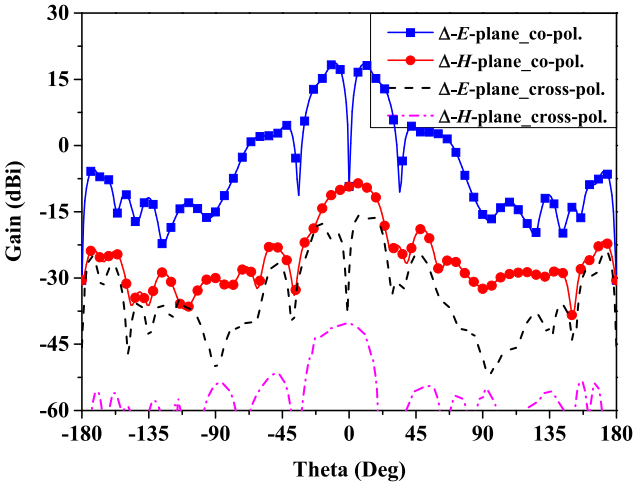

FIGURE 16. Measured difference-patterns of azimuth plane (*E*-plane) and elevation plane (*H*-plane) at 77 GHz.

2 dB lower. This value slightly deviates from the theoretical value of 3 dB, which is mainly due to the non-ideality of the developed MPC. And the null-depths are lower than −20 dB in the difference-patterns.

IV. BEAM SHARPENING PROCESSING

A. DUAL-CHANNEL DECONVOLUTION ANALYSIS

As mentioned above, the received signal in azimuth dimension can be considered as the convolution of the antenna pattern and the angle information of targets, therefore, the deconvolution method can be utilized in forward-looking imaging. The algorithm model is as follows.

Consider $f(k)$ is defined as the azimuth sampling sequence of the target reflectivity distribution function, the azimuth echo sequence of the target $g(k)$ can be written as

$$g(k) = f(k) * h(k) + n(k) \tag{3}$$

where $h(k)$ is the azimuth sampling sequence of antenna pattern, and $n(k)$ is the effect of noise. In the angular frequency domain, (3) is recast as

$$G(\omega) = F(\omega) \cdot H(\omega) + N(\omega) \tag{4}$$

where $G(\omega)$, $F(\omega)$, $H(\omega)$, and $N(\omega)$ represent the Fourier transform of $g(k)$, $f(k)$, $h(k)$ and $n(k)$, respectively. Thus the azimuth information of the target in the frequency domain can be given by

$$F(\omega) = \frac{G(\omega) - N(\omega)}{H(\omega)} \tag{5}$$

The corresponding azimuth echo sequences of the target (respectively denoted by $g_\Sigma(k)$ and $g_\Delta(k)$ can be expressed as

$$\begin{aligned} g_\Sigma(k) &= f(k) * h_\Sigma(k) + n_\Sigma(k) \\ g_\Delta(k) &= f(k) * h_\Delta(k) + n_\Delta(k) \end{aligned} \tag{6}$$

In equation (6), $n_{\Sigma}(k)$ and $n_{\Delta}(k)$ represent the added white Gaussian noise in sum and difference channels, respectively. If $h_{\Sigma}(k)$ and $h_{\Delta}(k)$ satisfy the strong coprime condition, then the corresponding deconvolution factor $d_{\Sigma}(k)$ and $d_{\Delta}(k)$ can be constructed and satisfy the following relationship,

$$h_{\sum}(k) * d_{\sum}(k) + h_{\Delta}(k) * d_{\Delta}(k) = \delta \tag{7}$$

where δ is the impulse function, and equation (6) can be rearranged as

$$\begin{aligned} g_{\sum}(k) * d_{\sum}(k) &= f(k) * h_{\sum}(k) * d_{\sum}(k) + n_{\sum}(k) * d_{\sum}(k) \\ g_{\Delta}(k) * d_{\Delta}(k) &= f(k) * h_{\Delta}(k) * d_{\Delta}(k) + n_{\Delta}(k) * d_{\Delta}(k) \end{aligned} \tag{8}$$

Furtherly, $f\ (k)$ can be derived and written as the following expression form,

$$\begin{aligned} f(k) = g_{\sum}(k) * d_{\sum}(k) + g_{\Delta}(k) * d_{\Delta}(k) \\ - [n_{\sum}(k) * d_{\sum}(k) + n_{\Delta}(k) * d_{\Delta}(k)] \end{aligned} \tag{9}$$

Equation (9) denotes the azimuth information of a target $f\ (k)$ can be retrieved based on the received echoes from sum and difference channels ($g_{\Sigma}(k)$ and $g_{\Delta}(k)$) and the two coprime deconvolution factor ($d_{\Sigma}(k)$ and $d_{\Delta}(k)$). Meanwhile, the channel noise $n_{\Sigma}(k)$ and $n_{\Delta}(k)$ also affect the recovery of target azimuth information.

In practical engineering applications, as long as the frequency response of each convolution factor is not equal to zero simultaneously, they are considered satisfy the coprime condition. Thus, the frequency domain deconvolution factors of sum and difference channels can be written as the following expression,

$$\begin{aligned} D_{\sum}(\omega) &= \frac{H_{\sum}(\omega)^*}{\left|H_{\sum}(\omega)\right|^2 + |H_{\Delta}(\omega)|^2} \cdot \phi(\omega) \\ D_{\Delta}(\omega) &= \frac{H_{\Delta}(\omega)^*}{\left|H_{\sum}(\omega)\right|^2 + |H_{\Delta}(\omega)|^2} \cdot \phi(\omega) \end{aligned} \tag{10}$$

where $H_{\Sigma}(\omega)^*$ and $H_{\Delta}(\omega)^*$ are complex conjugates of $H_{\Sigma}(\omega)$ and $H_{\Delta}(\omega)$, respectively, and $\phi(\omega)$ is defined as a filter function with corresponding impulse response in time domain. To reduce the influence of noise, 3dB beamwidth of the patterns are usually truncated for beam sharpening [33].

B. BEAM SHARPENING SIMULATION AND DISCUSSION

Based on the above mentioned algorithm model and measured sum- and difference-patterns in azimuth plane shown in Fig. 15 and Fig. 16, the performance of the proposed beam sharpening antenna is verified by simulation in this section.

In the following simulation, an ideal point scatter is set as the target $f\ (k)$, such as the impulse function $\delta(k)$ at a certain point. In this way, the received azimuth echo is just the real beam pattern of the sum channel. Because the real beam has a certain width, it looks as if the target $\delta(k)$ has been extended in azimuth. After deconvolution of sum and difference channels, the point target is expected to be restored, in other words, the real beam appears to be sharpened.

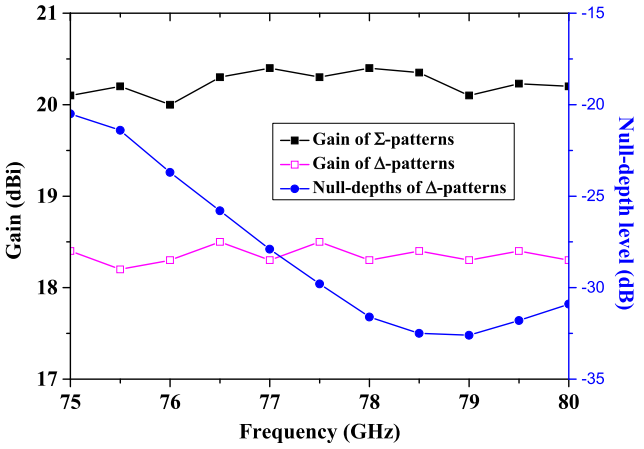

FIGURE 17. Measured gain and null-depth levels versus frequencies.

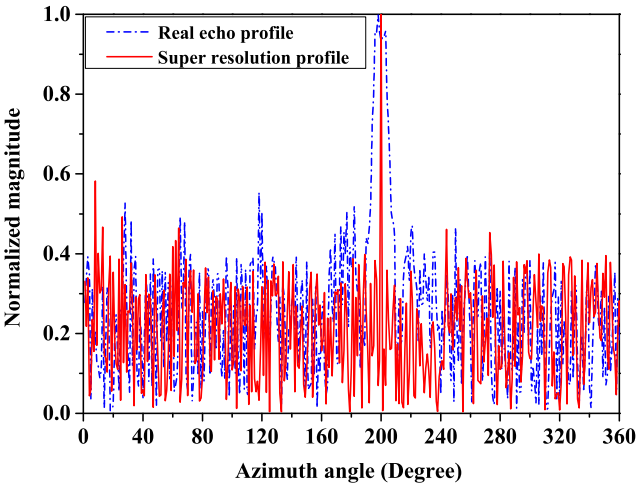

FIGURE 18. Simulation results of a single point target when the SNR is 0 dB.

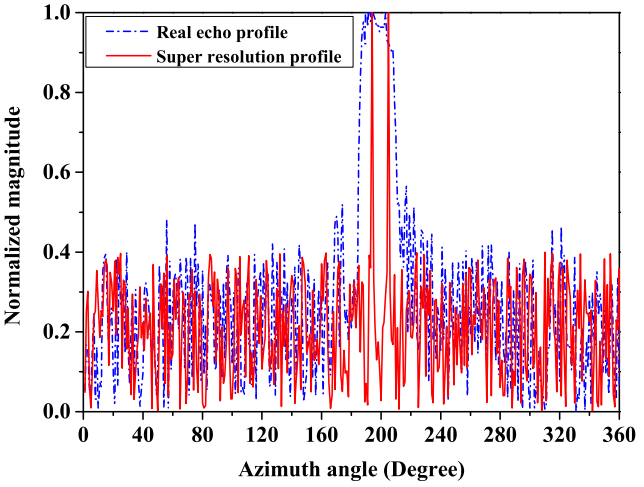

FIGURE 19. Simulation results of two close point targets when the SNR is 0 dB.

Suppose that a point target is located at the forward-looking region of the antenna, the azimuth angle of the point target is 200°. Fig. 18 shows the simulated real beam echo of the

sum channel at 77 GHz and the results processed by the beam sharpening when the SNR is 0 dB. The added noise obeys a zero mean Gaussian distribution. It is obviously the real beam echoes of the point target is extended in azimuth, thus the azimuth resolution is decreased. After the beam sharpening processing, the azimuth echoes of the point target is greatly compressed, and the sharpening ratio is about 12 dB with SNR of 0 dB and truncated 3dB beamwidth.

To further verify the ability of beam sharpening in azimuth compression more intuitively, it is assumed that there are two point targets with azimuth angles of 194° and 205°, respectively. The azimuth angle between the two point targets is 11°, which is slight less than the 12° HPBW of sum-pattern, just as shown in Fig. 15. Obviously, when two targets are in the range of a main beam simultaneously, it is difficult to distinguish them in azimuth without super-resolution. Fig. 19 shows the azimuth characteristics of two targets before and after beam sharpening, and the two close targets can be distinguished clearly compared to the real beam echoes without processing.

V. CONCLUSION

This paper takes the E-band front-looking real aperture radar as the application background, focusing on how to achieve high azimuth resolution through a small aperture receiving antenna. To this end, a monopulse antenna with coprime channels (sum channel and difference channel) is designed and measured in detail. Based on the measured sum- and difference-patterns data, a deconvolution based beam sharpening processing is implemented in digital domain, and simulation results show that the proposed antenna module and corresponding super-resolution processing significantly improve the azimuth resolution. In the follow-up research, the antenna module will be combined with transceiver and servo to carry out the actual imaging demonstration.

REFERENCES

[1] M. Na, P. Li, and Z. Zhou, "Sparse Fourier transform based millimeter wave wideband spectrum sensing," in *Proc. 11th Int. Conf. Wireless Commun., Netw. Mobile Comput.*, Shanghai, China, Sep. 2015, pp. 1–6.

[2] Z. Guizani and N. Hamdi, "MmWave E-band D2D communications for 5G-underlay networks: Effect of power allocation on D2D and cellular users throughputs," in *Proc. IEEE Symp. Comput. Commun. (ISCC)*, Messina, Italy, Jun. 2016, pp. 114–118.

[3] J. Senic, C. Gentile, P. B. Papazian, K. A. Remley, and J.-K. Choi, "Analysis of E-band path loss and propagation mechanisms in the indoor environment," *IEEE Trans. Antennas Propag.*, vol. 65, no. 12, pp. 6562–6573, Dec. 2017.

[4] B. Schoch, S. Chartier, U. Mohr, M. Koller, S. Klinkner, and I. Kallfass, "Towards a CubeSat mission for a wideband data transmission in E-band," in *Proc. IEEE Space Hardw. Radio Conf. (SHaRC)*, San Antonio, TX, USA, Jan. 2020, pp. 16–19.

[5] J. Montero-de-Paz, I. Oprea, V. Rymanov, S. Babiel, L. E. García-Muñoz, A. Lisauskas, M. Hoefle, A. Jimenez, O. Cojocari, D. Segovia-Vargas, A. Stöhr, and G. Carpintero, "E-band (71–76 GHz) wireless link using compact modules," *Electron. Lett.*, vol. 49, no. 7, pp. 476–477, Mar. 2013.

[6] J. Wenger, "Automotive mm-wave radar: Status and trends in system design and technology," in *Proc. IEE Colloq. Automot. Radar Navigat. Techn.*, London, U.K., Feb. 1998, pp. 1/1–1/7.

[7] J. Hasch, E. Topak, R. Schnabel, T. Zwick, R. Weigel, and C. Waldschmidt, "Millimeter-wave technology for automotive radar sensors in the 77 GHz frequency band," *IEEE Trans. Microw. Theory Techn.*, vol. 60, no. 3, pp. 845–860, Mar. 2012.

[8] W. M. Huang, J. P. John, S. Braithwaite, J. Kirchgessner, I. S. Lim, D. Morgan, Y. B. Park, S. Shams, I. To, P. Welch, R. Reuter, H. Li, A. Ghazinour, P. Wennekers, and Y. Yin, "SiGe 77 GHz automotive radar technology," in *Proc. IEEE Int. Symp. Circuits Syst.*, New Orleans, LA, USA, May 2007, pp. 1967–1970.

[9] T. Shi, Y. Gong, S. Ravichandran, V. Sundaram, J. D. Cressler, and R. Tummala, "Next generation of automotive radar with leading-edge advances in SiGe devices and glass panel embedding (GPE)," in *Proc. IEEE 68th Electron. Compon. Technol. Conf. (ECTC)*, San Diego, CA, USA, May/Jun. 2018, pp. 1245–1250.

[10] Z. Zhang, X. Di, Y. Xu, and J. Tian, "Concealed dangerous object detection based on a 77 GHz radar," in *Proc. IEEE Int. Workshop Electromagn., Appl. Student Innov. Competition*, Nagoya, Japan, Aug. 2018, pp. 1–2.

[11] Y. Wang, W. Wang, M. Zhou, A. Ren, and Z. Tian, "Remote monitoring of human vital signs based on 77-GHz mm-wave FMCW radar," *Sensors*, vol. 20, no. 10, pp. 1–23, May 2020.

[12] L. Li, R. Zhu, H. Li, and J. Zhou, "Human posture recognition based on multi-channel SAR at 77 GHz," in *Proc. IEEE 2nd Int. Conf. Autom., Electron. Electr. Eng.*, Shenyang, China, Nov. 2019, pp. 559–563.

[13] A. A. Belyaev, I. O. Frolov, T. A. Suanov, and D. O. Trots, "Object detection in an urban environment using 77 GHz radar," in *Proc. Radiat. Scattering Electromagn. Waves*, Divnomorskoe, Russia, Jun. 2019, pp. 436–439.

[14] J. Wang, X. Geng, and S. Wei, "Airport runway FOD detection system based on 77 GHz millimeter wave radar sensor," in *Proc. IEEE Int. Conf. Integr. Circuits, Technol. Appl.*, Chengdu, China, Nov. 2019, pp. 140–143.

[15] N. Ram, G. Hongmin, M. S. Sadiq, and A. C. Bahadur, "77 GHz corporate feed series microstrip antenna array for the applications of automotive radar," in *Proc. 9th Asia–Pacific Conf. Antennas Propag.*, Xiamen, China, Aug. 2020, pp. 1–2.

[16] X. Qiu, D. Hu, and C. Ding, "Some reflections on bistatic SAR of forward-looking configuration," *IEEE Geosci. Remote Sens. Lett.*, vol. 5, no. 4, pp. 735–739, Oct. 2008.

[17] W. Pu, W. Li, J. Wu, Y. Huang, J. Yang, and H. Yang, "An azimuth-variant autofocus scheme of bistatic forward-looking synthetic aperture radar," *IEEE Geosci. Remote Sens. Lett.*, vol. 14, no. 5, pp. 689–693, May 2017.

[18] G. Wang, L. Feng, J. Li, T. Xing, C. Ma, and C. Kang, "A robust image stitching and geometric correction method for Doppler beam sharpening imaging," in *Proc. 6th Asia–Pacific Conf. Synth. Aperture Radar*, Xiamen, China, Nov. 2019, pp. 1–4.

[19] Y. Zhang, Q. Zhang, D. Mao, Y. Zhang, Y. Huang, and J. Yang, "Super-resolution Doppler beam sharpening based on sparse covariance fitting," in *Proc. IEEE Radar Conf.*, Boston, MA, USA, Apr. 2019, pp. 1–4.

[20] G. Zhao, Y. Fu, and Z. Zhuang, "Imaging by root-MUSIC for forward looking radar with linear array," in *Proc. Int. Conf. Wireless Commun. Signal Process.*, Hangzhou, China, Oct. 2013, pp. 1–6.

[21] E. Zhao, F. Zhang, D. Zhang, and S. Pan, "Three-dimensional multiple signal classification (3D-MUSIC) for super-resolution FMCW radar detection," in *IEEE MTT-S Int. Microw. Symp. Dig.*, Guangzhou, China, May 2019, pp. 1–3.

[22] W. Li, M. Niu, Y. Zhang, Y. Huang, and J. Yang, "Super-resolution imaging of real-beam scanning radar base on accelerated maximum a posteriori algorithm," in *Proc. IEEE Int. Geosci. Remote Sens. Symp.*, Yokohama, Japan, Jul./Aug. 2019, pp. 3173–3176.

[23] H. Rahman, *Fundamental Principles of Radar*. Boca Raton, FL, USA: CRC Press, 2019. Accessed: Jun. 3, 2019. [Online]. Available: https://www.taylorfrancis.com/books/fundamental-principles-radar-habibur-rahman/10.1201/9780429279478

[24] Y. T. Lo and S. W. Lee, *Antenna Handbook Theory, Applications, and Design*. Boston, MA, USA: Springer, 2019. Accessed: Feb. 28, 2010. [Online]. Available: https://link.springer.com/book/10.1007/978-1-4615-6459-1/

[25] Y. Huang, Y. Zha, Y. Zhang, Y. Wang, and J. Yang, "Real-beam scanning radar angular super-resolution via sparse deconvolution," in *Proc. IEEE Geosci. Remote Sens. Symp.*, Quebec City, QC, Canada, Jul. 2014, pp. 3081–3084.

[26] R. Bose, A. Freedman, and B. D. Steinberg, "Sequence CLEAN: A modified deconvolution technique for microwave images of contiguous targets," *IEEE Trans. Aerosp. Electron. Syst.*, vol. 38, no. 1, pp. 89–97, Jan. 2002.

[27] Z. Deng, F. Zhang, M. Liang, Y.-L. Yao, and F. Zhang, "A dual-port sum-difference beam antenna with simple structure and very high isolation," *Prog. Electromagn. Res. C*, vol. 74, pp. 41–49, 2017.
[28] H. Chen, W. Che, Q. He, W. Feng, X. Wei, and K. Wu, "Compact substrate integrated waveguide (SIW) monopulse network for *Ku*-band tracking system applications," *IEEE Trans. Microw. Theory Techn.*, vol. 62, no. 3, pp. 472–480, Mar. 2014.
[29] M. Mohammadi and F. H. Kashani, "Planar eight port waveguide monopulse comparator," *Prog. Electromagn. Res. C*, vol. 6, pp. 103–113, 2009.
[30] Y. Chen, Y. Xu, L. Hu, W. Tong, and R. Xu, "A broadband passive monopulse comparator MMIC," *IEEE Microw. Wireless Compon. Lett.*, vol. 27, no. 4, pp. 359–361, Apr. 2017.
[31] T. Das and V. K. Singh, "Broadband waveguide monopulse comparator at X-band," in *Proc. IESC*, Shillong, India, Apr. 2017, pp. 181–185.
[32] J. Dittloff, F. Arndt, and D. Grauerholz, "Optimum design of waveguide E-plane stub-loaded phase shifters," *IEEE Trans. Microw. Theory Techn.*, vol. MTT-36, no. 3, pp. 582–587, Mar. 1988.
[33] Y. Zha, Y. Huang, Z. Sun, Y. Wang, and J. Yang, "Bayesian deconvolution for angular super-resolution in forward-looking scanning radar," *Sensors*, vol. 15, no. 3, pp. 6924–6946, Mar. 2015.

ZHENHUA CHEN (Member, IEEE) received the B.Sc. degree in information engineering and the M.Sc. degree in electromagnetic field and microwave technology from the Nanjing University of Aeronautics and Astronautics, Nanjing, China, in 2006 and 2009, respectively, and the Ph.D. degree in electromagnetic field and microwave technology from Southeast University, Nanjing, in 2014. He joined the School of Electronic and Information Engineering, Nanjing University of Information Science and Technology, Nanjing, as a Lecturer, in March 2014. His current research interests include millimeter wave and terahertz solid state circuits, antenna technologies, radio frequency transceivers, and near range radar applications.

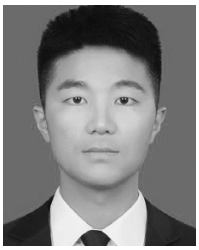

PENG TENG (Graduate Student Member, IEEE) was born in Jiangsu, China. He received the B.S. degree in electronic information engineering from the Huaiyin Institute of Technology, Huaian, China, in 2018. He is currently pursuing the M.S. degree in electronic and communication engineering with the Nanjing University of Information Science and Technology, Nanjing, China. His research interests include microwave antennas and microwave frequency synthesizers.

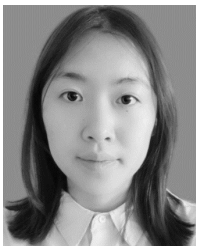

JIANRU WANG (Graduate Student Member, IEEE) was born in Jiangsu, China. She received the B.S. degree in electronic information engineering from the Nanhang Jincheng College, Nanjing, China, in 2019. She is currently pursuing the M.S. degree in electronic and communication engineering with the Nanjing University of Information Science and Technology, Nanjing. Her research interests include microwave passive devices, dielectric oscillators, and microwave self-oscillating mixers.